Nanoscale

Accepted Manuscript

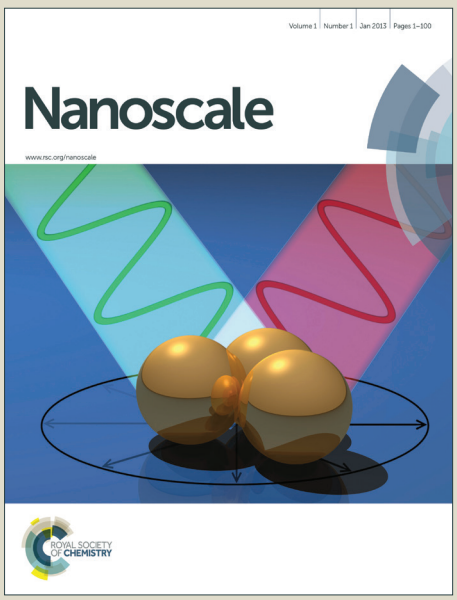

ROYAL SOCIETY OF CHEMISTRY

www.rsc.org/nanoscale

Cite this: DOI: 10.1039/c0xx00000x

www.rsc.org/xxxxxx

ARTICLE TYPE

Controllable Synthesis of Porous Fe_3O_4@ZnO Spheres Decorated Graphene for Extraordinary Electromagnetic Wave Absorption

Danping Sun, Quan Zou, Yanping Wang, Yujiao Wang, Wei Jiang* and Fengsheng Li

Received (in XXX, XXX) Xth XXXXXXXXX 20XX, Accepted Xth XXXXXXXXX 20XX

DOI: 10.1039/b000000x

For the first time, mesoporous Fe_3O_4@ZnO spheres decorated graphene (GN- *p* Fe_3O_4@ZnO) composites with uniform size, considerable porosity, high magnetization and extraordinary electromagnetic (EM) wave absorption properties were synthesized by a simple and efficient three-step method. Structure and morphology details were characterized by X-ray diffraction, transmission electron microscopy, high-resolution electron microscopy and field-emission scanning electron microscopy. Electron microscopy images reveal that *p* Fe_3O_4@ZnO spheres with obvious porous and core-shell structures are uniformly coated on both sides of GN sheets without significant vacancy or apparent aggregation. EM wave absorption properties of epoxy containing 30 *wt* % GN- *p* Fe_3O_4@ZnO were investigated at room temperature in the frequency region of 0.2~18 GHz. The absorption bandwidth with the reflection loss (RL) values less than –10 dB is up to 11.4 GHz, the minimal RL is almost –40 dB. The intrinsic of physical and chemical properties of materials, the synergy of Fe_3O_4 and ZnO, and particularly the unique multi-interfaces are fundamental to the enhancement of EM absorption properties. The as-prepared GN-*p* Fe_3O_4@ZnO composites are shown to be lightweight, strong absorption, and broad frequency bandwidth EM absorbers.

1. Introduction

Electromagnetic (EM) wave radiations arising from the rapid progress of wireless telecommunication technology have attracted great interests in exploiting different kinds of EM absorption materials to eliminate these unwanted EM wave pollutions.[1-4] Excellent EM wave absorption materials are requested to be light weight, strong absorption, high thermal stability as well as broad absorption frequency bandwidth.[5] The traditional absorber, Fe_3O_4, has strong absorption properties and low cost, thus showing great potential as high-performance EM wave absorbers.[6] However, the pure Fe_3O_4 absoebers usually exhabit a very narrow absorption frequency bandwidth (mainly distributes in low-frequency range), and the required addition amount is over 50 *wt* % to get the best absorbance of EM waves. The high weight density and a large disparity of permittivity and permeability limit its progress in scalable application.[7] Therefore, many kinds of hybrids of magnetic metals, conducting polymer, carbon and dielectric materials have been explored to improve the balance between permittivity and permeability.[8-11] Core-shell structured composites, i.e., Fe_3O_4@SiO_2, Fe_3O_4@Ni-B, Fe_3O_4@TiO_2 Fe_3O_4@C nanoparticles with new or enhanced EM absorption properties compared to the naked Fe_3O_4 have been reported previously.[12-15]

Considering the superior magnetic properties of Fe_3O_4 and dielectric properties of ZnO, it is feasible to coat the Fe_3O_4 nanoparticles with a ZnO nanoshell, which will take an advantage of the superior properties of the two components. Many researches focusing on this area revealed that the combination of Fe_3O_4 and ZnO resulted in an increase of the impedance matching as well as greatly enhanced their EM absorption performance.[7,16,17] To our best knowledge, there is no report on the controlled synthesis of Fe_3O_4@ZnO with porous structure. Herein, we designed and synthesized a hybrid of porous Fe_3O_4 core, ZnO nanoshell, and graphene (GN) substrate, which will be called porous Fe_3O_4@ZnO-decorated GN (GN- *p* Fe_3O_4@ZnO) in following. Compared with the normal Fe_3O_4@ZnO composites,[16] four extra unique advantages were observed apart from the increase of the impedance matching. Multi-interfaces existing in the composites result in a significant interfacial polarization, which would have important effect on the increase of dielectric loss. The GN sheets serve as an ideal substrate for the deposition of the *p* Fe_3O_4@ZnO spheres to prevent their aggregations, which could improve the attenuation efficiency of EM wave energies. Furthermore, the residual defects and the excellent electron transport property of GN sheets can introduce charge polarization and electronic dipole relaxation. Finally, the GN is well known lightweight, it could decrease the density of the composites. Therefore, we consider GN- *p* Fe_3O_4@ZnO composites as high-performance and light weight EM wave absorption materials.

The above designed composites were fabricated by a controllable three-step method, illustrated in Fig. 1. As shown in the Fig. 1, *p* Fe_3O_4 nanoparticles were prepared by a simple hydrothermal route using a complex polylol system as solvent,

and modified GN dispersion was obtained by the exfoliation and reduction of graphite oxide (GO) in the presence of sodium dodecylbenzenesulfonate. Then, ZnO nanocrystal shell was coated on *p* Fe_3O_4 by a simple sol-gel method.[18] Finally, the electropositive *p* Fe_3O_4@ZnO spheres attached to the negative charged GN sheets through electrostatic interaction.[19] Comparing with the reported one-pot deposition, [20-23] the preparation of *p* Fe_3O_4@ZnO spheres and the deposition occur step by step, making the process more controllable. Moreover, we obtained the highly porous and monodispersed *p* Fe_3O_4 nanoparticles using complex polylol system without any adamant or soft template, which requires less post-treatments.[24] The morphology, structure, magnetic and porosity properties were investigated in detail, a multiple absorbing mechanism was proposed to explain the excellent EM wave absorption properties of the as-prepared GN-*p* Fe_3O_4@ZnO composites.

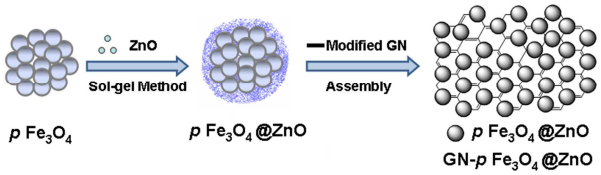

Fig. 1. Illustration for the three-step synthesis of GN-*p* Fe_3O_4@ZnO.

2. Experimental Section

Materials. Ferric chloride hexahydrate ($FeCl_3 \cdot 6H_2O$), sodium acetate (NaAc), zinc acetate dihydrate ($Zn(Ac)_2 \cdot 2H_2O$), sodium hydroxide (NaOH), polyethylene glycol (PEG, $M_W = 4000$), EG, and PG were obtained from Aldrich. GO used in this work was prepared from nature graphite powder (Nanjing JCNO Tech Co., Ltd) according to Hummers method.[25] All chemicals in this experiment are analytical grade and used as received without further purification.

Synthesis of GN-*p* Fe_3O_4@ZnO composites. The composites were fabricated by a three-step process: (1) *p* Fe_3O_4 nanoparticles were prepared by a simple hydrothermal route using a complex polylol system as solvent, and modified GN dispersion was obtained by the exfoliation and reduction of GO,[26-28] the detailed synthesis process was described in our previous report.[29] (2) *p* Fe_3O_4@ZnO core-shell structured spheres were synthesized by a simple sol-gel method. Typically, 0.1 g of above *p* Fe_3O_4 nanoparticles was dispersed in 100 mL of ethanol solution containing 1.20 g of $Zn(Ac)_2 \cdot 2H_2O$ and kept ultrasonic treatment for 10 min. Subsequently, the mixture was transferred to a flask and 25 mL of 0.25 M NaOH was dropped into it when the reaction temperature elevated to 40 ℃. The reaction was maintained for 4 h. The black precipitate was easily collected by a magnet, and washed for several times by ethanol. (3) Finally, the obtained *p* Fe_3O_4@ZnO spheres were mixed with 20 mL of modified GN dispersion and kept stirring for 24 h, the as-prepared GN-*p* Fe_3O_4@ZnO composites also can be collected by a magnet, and dried at 60℃ for 3 h.

Characterization. The structural characterization of GN-*p* Fe_3O_4@ZnO was carried out by powder X-ray diffraction (XRD) performed on a Bruker D8 Advance system by using Cu K_α radiation ($\lambda = 1.5418$ Å). X-ray photoelectron spectroscopy (XPS) was recorded on ESCALAB 250 photoelectron spectrometer. Transmission electron microscopy (TEM: Tecnai 12), high-resolution electron microscopy (HRTEM: Tecnai G2 F30 S-TWIN) and field-emission scanning electron microscopy (FE-SEM: Hitachi S-4800) were used to observe the morphologies of the products. Nitrogen (N_2) adsorption-desorption measurement was performed on a Micromertics ASAP 2020 system. Specific surface area was calculated by the Brunauer-Emmett-Teller (BET) method. The magnetic properties were measured at room temperature on a Lake Shore 7410 vibrating sample magnetometer. The composites used for EM absorption measurement were prepared by mixing the epoxy with 30 *wt* % GN-*p* Fe_3O_4@ZnO. The mixtures were then pressed into toroidal-shaped samples (φ_{out}: 7.00 mm, φ_{in}: 3.04 mm). The complex permittivity and permeability of the composites were measured by Agilent E8363A vector network analyzer in the frequency range of 0.2~18 GHz.

3. Results and Discussion

3.1 Morphology and structure

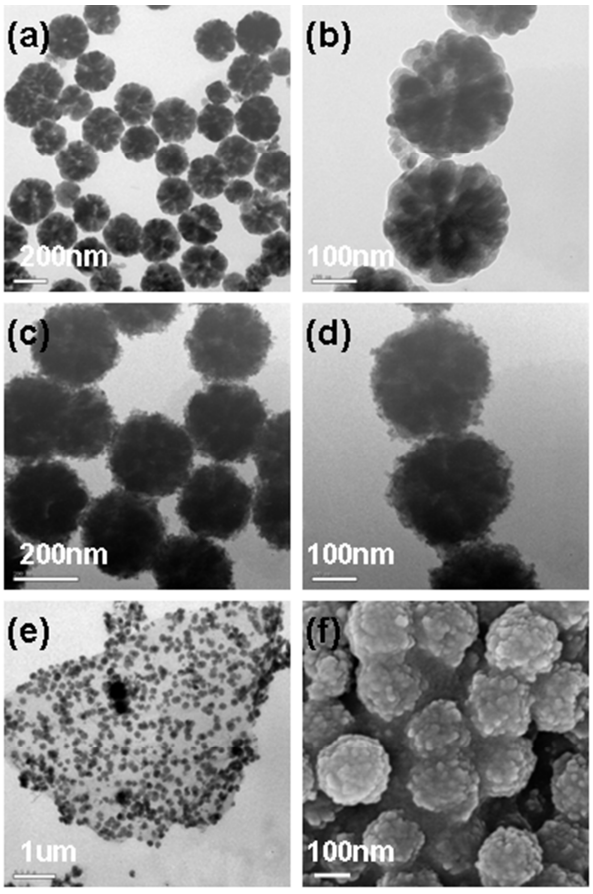

Fig. 2. TEM images of the products in different stages (a), (b) *p* Fe_3O_4, (c), (d) *p* Fe_3O_4@ZnO, (e) GN-*p* Fe_3O_4@ZnO and (f) corresponding FE-SEM image.

The reduction process of GO was proved by XPS spectra which is shown in Fig. S1. The C_{1s} XPS spectrum confirms a considerable degree of reduction. The sizes and morphologies of the products in different stages were characterized by TEM and

FE-SEM. Fig. 2a, b show the TEM images of *p* Fe_3O_4 nanoparticles in different magnifications. It is evident that the *p* Fe_3O_4 nanoparticles are approximately monodispersed with a mean diameter of ~200 nm. The existing pale and dark regions of the nanoparticles suggest their porous structures.[30] In Fig. 2b, it can be clearly observed that the porous nanoparticles are composed of irregular shaped nanoparticles. The corresponding FE-SEM image (Fig. S2) confirms again that the *p* Fe_3O_4 nanoparticles consist of some small nanocrystals with a rough surface, and several obvious pores can be found which are in accordance with the TEM results. After the coating of ZnO layer, the diameter of the *p* Fe_3O_4@ZnO spheres increases by around 30 nm (Fig. 2c) and the spheres maintain a rough surface as the coating layer consists of many small ZnO nanocrystals (Fig. 2d). In comparison of *p* Fe_3O_4, it is noteworthy that the blacker core of *p* Fe_3O_4@ZnO and disappearance of pale regions also confirm the coating of ZnO shell. Fig. 2e presents the typical *p* Fe_3O_4@ZnO spheres decorated GN composites, each GN sheet is well decorated by a large quantity of uniform *p* Fe_3O_4@ZnO spheres, and there is no large area of the GN sheet without *p* Fe_3O_4@ZnO decoration and no individual *p* Fe_3O_4@ZnO sphere outside of the GN sheet. Furthermore, the corresponding FE-SEM image (Fig. 2f) shows the spheres coated on GN are also composed of nanocrystals with a rough surface like *p* Fe_3O_4 nanoparticles but of smaller size, which are also in accordance with the TEM results. As the *p* Fe_3O_4@ZnO coated on both sides of the GN sheet like a sandwich, the GN sheet can't be seen directly, the white line in Fig. S3 indexes the position of it, implying the GN sheet is still flexible even after the coating.

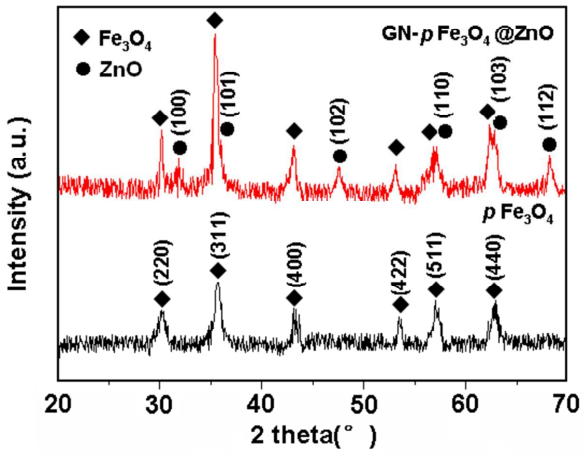

Fig. 3. XRD patterns of *p* Fe_3O_4 and GN- *p* Fe_3O_4@ZnO composites.

The composition and crystallinity of the fabricated composites were investigated by XRD. As shown in Fig. 3, there are six major diffraction peaks at 30.00°, 35.45°, 43.10°, 53.44°, 57.04° and 62.68° observed for the *p* Fe_3O_4 nanoparticles, which can be well indexed to (220), (311), (400), (422), (511) and (440) planes of the pure face-centered cubic structured Fe_3O_4 (JCPDS No. 19-0629), respectively. In the case of GN- *p* Fe_3O_4@ZnO composites, the peaks of cubic magnetite still exist, revealing that the *p* Fe_3O_4 nanoparticles do not change their phase after the coating process. Besides, six extra diffraction peaks arising from ZnO, which may be properly indexed to the hexagonal ZnO phase (JCPDS No. 36-1451). In addition, there is no obvious diffraction peak attributed to graphite observed, indicating that the stacking of GN sheets remained disordered.

The detail of the core-shell structure was further characterized by HRTEM. As shown in Fig. 4a, the clear interface is presented between Fe_3O_4 core and ZnO shell, indicating the heterojunction formed at the interface. The lattice planes of the core region are measured to be 0.293 and 0.253 nm, corresponding to the spacing of (220) and (311) planes of Fe_3O_4, respectively. As well, the lattice planes at the edge are 0.281 and 0.162 nm, coresponging to the (100) and (110) planes of ZnO (Fig. 4b). Moreover, the peaks of O, Fe, and Zn elements are presented in the energy dispersive spectroscopy (EDS) spectrum (Fig. 4c), confirming the exsitence of ZnO. Fig. 4d is the elemental mapping of Fe, O and Zn corresponding to the *p* Fe_3O_4@ZnO sphere (D ~ 230 nm). The images labeled Fe, O and Zn are uniform along the shape of sphere, revealing that *p* Fe_3O_4 particles are coated by ZnO homogenously.

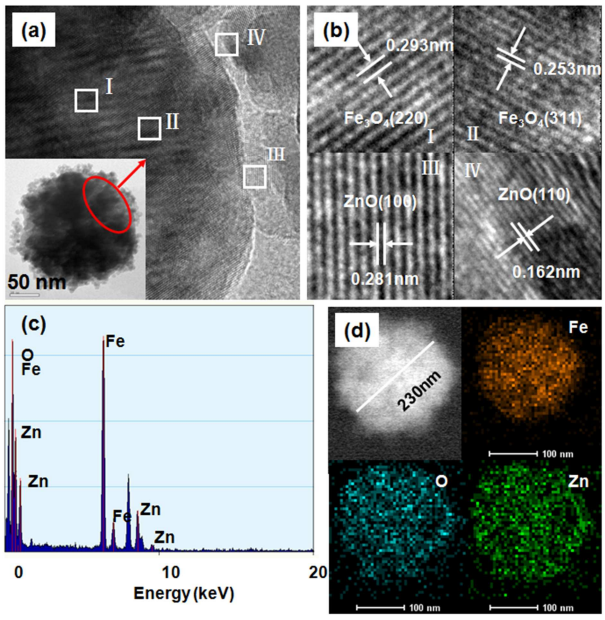

Fig. 4. (a), (b) HRTEM images, (c) EDS spectrum and (d) elemental mapping of Fe, O, Zn of *p* Fe_3O_4@ZnO spheres.

All above reveal that GN- *p* Fe_3O_4@ZnO composites are successfully fabricated by the present method. In our previous work, Fe_3O_4 nanoparticles with different sizes and microstructures were obtained using different complex polylol solvents.[29] Besides, it is feasible to control the thickness of ZnO layer by the concentration of zinc precursor.[31] As a result, the size, microstructure and thickness of ZnO layer can be tailored by this three-step method, indicating that the physical and chemical properties of the GN- *p* Fe_3O_4@ZnO composites can be tailored for different applications.

3.2 Magnetic and porosity property

The magnetic properties of the fabricated GN- *p* Fe_3O_4@ZnO composites were examined at room temperature on a magnetometer compared with pure *p* Fe_3O_4. The magnetization

curves in Fig. 5 show that the *p* Fe_3O_4 has a high magnetization saturation (M_S) value of 82.18 emu g^{-1} , which is close to its bulk value (92 emu g^{-1}).[32] The value of M_S decreases from 82.18 to 72.06 emu g^{-1} as ZnO is coated as well as the GN is added. This decrease in magnetism is mainly attributed to the decrease in weight ratio of *p* Fe_3O_4. The coercive fields observed in insert (a) of Fig. 5 can be due to the aggregation of small Fe_3O_4 nanocrystals and the presence of ZnO nanoparticles.[33] The obtained GN- *p* Fe_3O_4@ZnO composites can be easily collected by a permanent magnet (insert (b) of Fig. 5), even after a long time of sonication, the *p* Fe_3O_4@ZnO spheres were still firmly anchored on the surface of GN uniformly, indicating the strong interaction between the two substances. The porosity of the *p* Fe_3O_4 nanoparticles was further substantiated by the N_2 sorption measurement. The N_2 adsorption-desorption isotherm curve can be identified as type IV, which is characteristic of mesopores (Fig. S4). The BET surface area of the sample was calculated to be 22.23 m^2 g^{-1}, which is much higher than the value (2.89 m^2 g^{-1}) of dense spheres with the similar diameter. All data strongly support the existence of porous structure of the spheres.

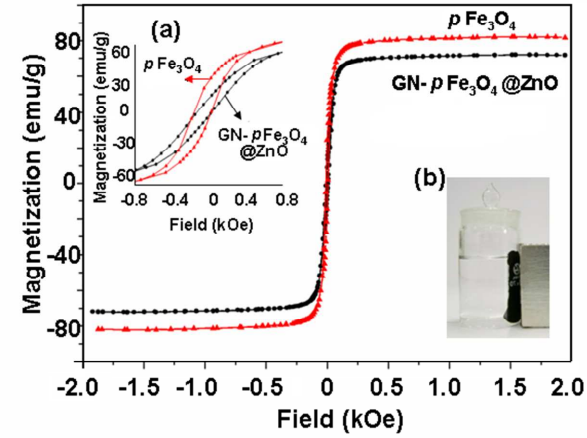

Fig. 5. Magnetization curves of *p* Fe_3O_4 and GN- *p* Fe_3O_4@ZnO. Insert (a) *M vs. H* plot in a low field region, insert (b) typical magnetic separation of the composites dispersed in water.

3.3 EM absorption property

According to the transmit-line theory,[34] the absorbing characteristics of the materials depend on the frequency, sample thickness, relative complex permittivity ($\varepsilon_r = \varepsilon' - j\varepsilon''$), relative complex permeability ($\mu_r = \mu' - j\mu''$) and so on. In order to investigate the effects on the EM wave absorption in the present material systems, the EM parameters of epoxy containing 30 *wt* % GN- *p* Fe_3O_4@ZnO composites were measured at room temperature in the frequency range of 0.2~18 GHz. The EM wave absorption properties, denoted by the reflection loss (RL), can be calculated by the following equations:

$$Z_{in} = (\mu_r/\varepsilon_r)^{1/2} \tanh\left[j(2\pi fd/c)(\mu_r\varepsilon_r)^{1/2}\right] \quad (1)$$

$$RL(dB) = 20\log\left|\frac{Z_{in}-1}{Z_{in}+1}\right| \quad (2)$$

where Z_{in} is the input impedance of the absorber, μ_r and ε_r are the relative complex permeability and permittivity, f is the frequency of EM waves, d is the thickness of the absorber, and c is the velocity of EM waves in free space.

The calculated RL of the GN- *p* Fe_3O_4@ZnO composites with different thicknesses according to the above equations are shown in Fig. 6. It is observed that the composites exhibit a certain extent abilities for EM wave absorption with the thicknesses in the range of 1~5 mm. Noticeably, a more stronger RL peak is observed at high-frequency besides of the normal RL peak at low-frequency in most magnetic absorbers. The strong ansorbance at high-frequency is attributed to the increase of dielectric loss.[29] Both of them have a tendency to shift from high-frequency to low-frequency and the values of minimal RL decrease with the increase of thickness. Importantly, the absorption bandwidth corresponding to RL < –10 dB (over 90% EM wave absorption) is almost up to 11.4 GHz (3.0~6.8 GHz, 10.4~18.0 GHz), and the minimal RL is almost –40 dB. Therefore, the GN- *p* Fe_3O_4@ZnO composites show better EM absorption properties in comparison with other magnetic materials such as GN/Fe_3O_4@Fe/ZnO, Fe_3O_4/carbon, and Fe_3O_4/SiO_2 composites.[17,35,36]

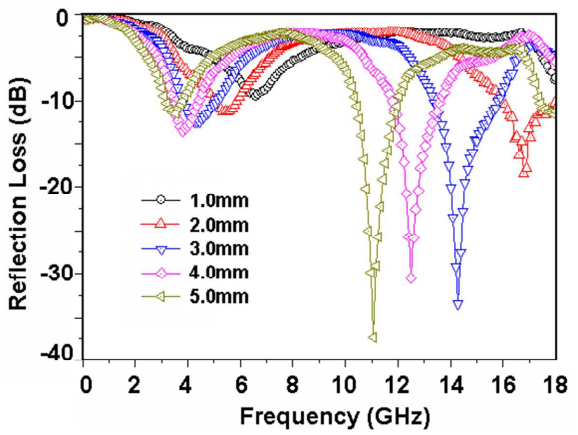

Fig. 6. Reflection loss of GN- *p* Fe_3O_4@ZnO composites with thickness 1~5 mm.

In our previous work, we have certified that the porous structure of Fe_3O_4 nanoparticles has an enhanced dielectric loss against EM waves which is the fundamental condition for the great improvement of EM absorption properties. In this present GN- *p* Fe_3O_4@ZnO system, the addition of ZnO as well as the core-shell structure enhanced EM absorption properties even more which could be attributed to the following two main aspects: (1) The efficient complementarities between the dielectric losses and the magnetic losses. As we all known that the EM absorption is strongly dependent on the complementarities between the dielectric loss and the magnetic loss.[2,4] When Fe_3O_4 nanoparticles are utilized alone, a large disparity of permittivity and permeability damages impedance matching, which results in a reduction of their EM absorption ability. For the GN- *p* Fe_3O_4@ZnO composites, *p* Fe_3O_4 nanoparticles are used as magnetic loss absorbers and ZnO nanoshell are used as dielectric loss absorbers. And the GN sheets serve as an ideal substrate for the deposition of the spheres to prevent their aggregations.[21] All above result in an improved impedance matching of the GN-

p Fe_3O_4@ZnO composites. (2) The extra interfacial polarization induced by porous and core-shell structures. Due to the porous structure of Fe_3O_4 nanoparticles, there are innumerable interfaces of Fe_3O_4-Fe_3O_4. Besides, three other kinds of material interfaces, i.e., Fe_3O_4-ZnO, ZnO-ZnO, and ZnO-GN, present simultaneously in the GN- *p* Fe_3O_4@ZnO composites. These multi-interfaces existing in the composites result in significant interfacial polarization, which would enhance the dielectric loss obviously at high frequency range.[17]

In general, the GN- *p* Fe_3O_4@ZnO composites fabricated in our work show extraordinary EM absorption properties over the frequency region of 0.2~18 GHz. Besides of the intrinsic of physical and chemical properties of materials, the synergy of different components and special design of structure are fundamental to the enhancement of EM absorption properties. The dielectric properties of such a heterogeneous composite arise due to the interfacial polarization and its associated relaxation. Additionally joule-heating loss is also expected due to conducting nature of GN. This multiple absorbing mechanism leads to a greatly improved EM absorption properties of materials.

4. Conclusions

In conclusion, the GN- *p* Fe_3O_4@ZnO composites with uniform size, porous and core-shell structures can be successfully prepared by the present method. All the core-shell structured *p* Fe_3O_4@ZnO spheres are homogeneously coated on both sides of GN sheets without significant vacancy or apparent aggregation. The as-prepared GN- *p* Fe_3O_4@ZnO composites show enhanced EM absorption properties over 0.2~18 GHz. The absorption bandwidth with the RL values less than –10 dB is up to 11.4 GHz, with the minimal RL is almost –40 dB. It indicates that more than 90% of EM wave energy could be attenuated by the composites. Moreover, the addition amount of the composites in the matrix is only 30 *wt* %. The multiple absorbing mechanism including the synergy of different components and interfacial polarization is fundamental to the enhancement of EM absorption properties. Our results demonstrate that GN- *p* Fe_3O_4@ZnO composites are very promising for the applications in lightweight, strong absorption, as well as broad absorption frequency bandwidth EM absorbers. Besides, the size, microstructure and thickness of ZnO layer can be tailored by this present synthesis method, indicating that the physical and chemical properties of the GN- *p* Fe_3O_4@ZnO composites can be tailored for other different applications.

Acknowledgments

This work is supported by the National Natural Science Foundation of China (50972060), the Fundamental Research Funds for the Central Universities (30920130112003), and the Weapon Research Support Fund (62201070804).

Notes and references

National Special Superfine Powder Engineering Research Center, Nanjing University of Science and Technology, Nanjing 210094, China. Fax: +86 25 84315942; Tel: +86 25 84315042; E-mail: weij_nust2013@yahoo.com(W. Jiang); sharly.sun2013@yahoo.com(D. Sun).

† Electronic Supplementary Information (ESI) available: [The C_{1s} XPS spectrum of GO and GN, FE-SEM images of *p* Fe_3O_4 nanoparticles and GN- *p* Fe_3O_4@ZnO composites, N_2 adsorption-desorption isotherm curve of the *p* Fe_3O_4 nanoparticles]. See DOI: 10.1039/b000000x/

1 A. K. Dhami, *Environ. Monit. Assess.,* 2011, **184,** 6507.
2 A. N. Yusoff, M. H. Abdullah, S. H. Ahmad, S. F. Jusoh, A. A. Mansor, S. A. A. Hamid, *J. Appl. Phys.,* 2002, **92,** 876.
3 C. M. Watts, X. Liu, W. Padilla, *J. Adv. Mater.,* 2012, **24,** OP98.
4 R. Che, L. Peng, X. Duan, Q. Chen, X. Liang, *Adv. Mater.,* 2004, **16,** 401.
5 T. Liu, P. Zhou, J. Xie, L. Deng, *J. Appl. Phys.,* 2012, **111,** 093905.
6 F. Wang, J. Liu, J. Kong, Z. Zhang, X. Wang, M. Itoh, K. Machida, *J. Mater. Chem.,* 2011, **21,** 4314.
7 Z. Wang, L. Wu, J. Zhou, B. Shen, Z. Jiang, *RSC Adv.,* 2013, **3,** 3309.
8 S. M. Abbas, M. Chandra, A. Verma, R. Chatterjee, T. C. Goel, *Compos. Part A,* 2006, **37,** 2148.
9 X. Bai, Y. Zhai, Y. Zhang, *J. Phys. Chem. C,* 2011, **115,** 11673.
10 Y. Zhan, F. Meng, Y. Lei, R. Zhao, J. Zhong, X. Liu, *Mater. Lett.,* 2011, **65,** 1737.
11 H. Yu, T. Wang, B. Wen, M. Lu, Z. Xu, C. Zhu, Y. Chen, X. Xue, C. Sun, M. Cao, *J. Mater. Chem.,* 2012, **22,** 21679.
12 Y. Deng, D. Qi, C. Deng, X. Zhang, D. Zhao, *J. Am. Chem. Soc.,* 2008, **130,** 28.
13 X. Li, X. Han, Y. Tan, P. Xu, *J. Alloy. Compd.,* 2008, **464,** 352.
14 J. Liu, R. Che, H. Chen, F. Zhang, F. Xia, Q. Wu, M. Wang, *Small,* 2012, **8,** 1214.
15 Y. Chen, G. Xiao, T. Wang, Q. Ouyang, L. Qi, Y. Ma, P. Gao, C. Zhu, M. Cao, B. Jin, *J. Phys. Chem. C,* 2011, **115,** 13603.
16 Y. Chen, F. Zhang, G. Zhao, X. Fang, H. Jin, P. Gao, C. Zhu, M. Cao, G. Xiao, *J. Phys. Chem. C,* 2010, **114,** 9239.
17 Y. Ren, H. Wu, M. Lu, Y. Chen, C. Zhu, P. Gao, M.; Cao, C. Li, Q. Ouyang, *ACS Appl. Mater. Inter.,* 2012, **4,** 6436.
18 F. Wang, J. Liu, X. Wang, J. Kong, S. Qiu, *Ceram. Int.* 2012, **38,** 6899.
19 G. Zhu, Y. Liu, Z. Xu, T. Jiang, C. Zhang, X. Li, G. Qi, *ChemPhysChem,* 2010, **11,** 2432.
20 S. Bai, X. Shen, X. Zhong, Y. Liu, G. Zhu, X. Xu, K. Chen, *Carbon,* 2012, **50,** 2337.
21 H. Cong, J. He, Y. Lu, S. Yu, *Small,* 2010, **6,** 169.
22 X. Li, X. Huang, D. Liu, X. Wang, S. Song, L. Zhou, H. Zhang, *J. Phys. Chem. C,* 2011, **115,** 21567.
23 C. Nethravathi, T. Nisha, N. Ravishankar, C. Shivakumara, M. Rajamathi, *Carbon,* 2009, **47,** 2054.
24 S. Xuan, F. Wang, J. M. Y. Lai, K. W. Y. Sham, Y. X. J. Wang, S. F. Lee, J. C. Yu, C. H. K. Cheng, K. C. F. Leung, *ACS Appl. Mater. Inter.,* 2011, **3,** 237.
25 S. William, J. R. Hummers, R. E. Offema, *J. Am. Chem. Soc.,* 1958, **80,** 1339.
26 S. Stankovich, D. A. Dikin, R. D. Piner, K. A. Kohlhaas, A. Kleinhammes, Y. Jia, Y. Wu, S. T. Nguyen, R. S. Ruoff, *Carbon,* 2007, **45,** 1558.
27 S. Park, R. S. Ruoff, *Nat. Nanotechnol.,* 2009, **4,** 217.
28 D. R. Dreyer, S. Park, C. W. Bielawski, R. S. Ruoff, *Chem. Soc. Rev.,* 2010, **39,** 228.
29 D. Sun, Q. Zou, G. Qian, C. Sun, W. Jiang, F. Li, *Acta Mater.,* 2013, **61,** 5829.
30 K. Cheng, S. Peng, C. Xu, S. Sun, *J. Am. Chem. Soc.,* 2009, **131,** 10637.
31 W. Wu, S. Zhang, X. Xiao, J. Zhou, F. Ren, L. Sun, C. Jiang, *ACS Appl. Mater. Inter.,* 2012, **4,** 3602.
32 H. Xu, M. Shao, T. Chen, S. Zhuo, C. Wen, M. Peng, *Micropor. Mesopor. Mat.,* 2012, **153,** 35.
33 A. Hasanpour, M. Niyaifar, M. J. Asan, J. J. Amighian, *Magn. Magn. Mater.,* 2013, **334,** 41.
34 P. Miles, W. Westphal, H. A. Von, *Rev. Mod. Phys.,* 1957, **29,** 279.
35 S. Ni, X. Wang, G. Zhou, F. Yang, J. Wang, D. He, *J. Alloy. Compd.,* 2010, **489,** 252.
36 M. Cao, X. Shi, X. Fang, H. Jin, Z. Hou, W. Zhou, *Appl. Phys. Lett.,* 2007, **91,** 203110.